Three-Dimensional Magnetic Tracking of Biaxial Sensors

Eugene Paperno and Pavel Keisar

Abstract—We present an analytical (noniterative) method for tracking biaxial magnetic sensors. Low-resolution regions (LRRs) of a biaxial transmitter are determined for the tracking of a triaxial sensor. These regions represent the *reciprocal* LRRs of a *biaxial* sensor that is tracked with a triaxial transmitter. The LRRs' configuration suggests that at least four triaxial transmitters should be used to track a biaxial sensor. At least one of the transmitters will always avoid the sensor's reciprocal LRRs. We show, on the other hand, that there are no LRRs for estimations of distance between the transmitter and the sensor. This makes it possible to triangulate a biaxial sensor with a triad of transmitters, instead of four. Thanks to a better distance resolution, compared to the resolution of coordinates, the triangulation provides practically the same location resolution and update rate as those reached by conventional methods of tracking triaxial sensors. This is true despite the need to operate a greater number of transmitting coils.

Index Terms—Biaxial sensor, distance resolution, location resolution, low-resolution region, magnetic tracking, reciprocal problem.

I. INTRODUCTION

RECENT applications of high-speed magnetic tracking such as intrabody navigation of medical instruments [1] and eye tracking [2] can benefit from employing subminiature magnetic sensors. A magnetic tracking sensor can radically be simplified and miniaturized if the number of its axes is reduced from three to two (see Fig. 1). Such simplification can also pave the way for introducing flat, completely integrated, solid-state sensors to magnetic tracking.

Triaxial sensors currently employed in high-speed, noniterative magnetic tracking are rather bulk ($\sim$100 mm^3) and complex [1]. Such sensors typically consist of three concentric orthogonal induction coils. It is difficult to combine three concentric coils in a single miniature device. It is even more difficult to achieve a good orthogonality of the subminiature coil assembly.

Biaxial solid-state sensors are technologically much simpler, more miniature, and geometrically precise. For instance, nonencapsulated solid-state sensors based on anisotropic magnetoresistance (AMR) or giant magnetoresistance (GMR) occupy less than a 2 mm^3 volume. Microlithography provides precise orthogonality to the solid-state sensors.

Compared to uniaxial sensors, biaxial sensors can be tracked with the help of fast noniterative algorithms. Biaxial sensors also
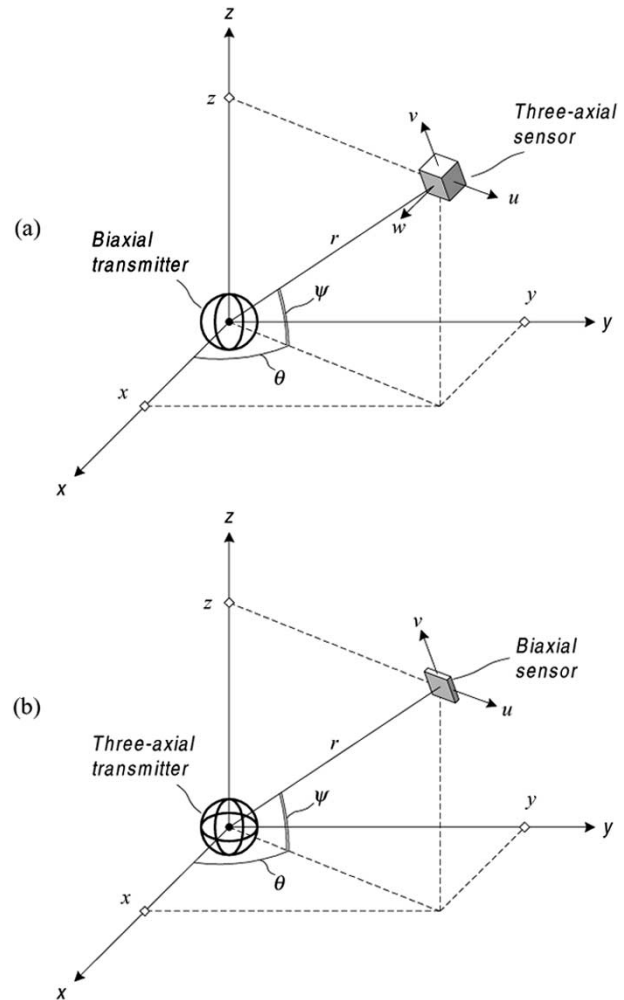
Fig. 1. Magnetic tracking. (a) The triaxial sensor is tracked with the biaxial transmitter. (b) The biaxial sensor is tracked with the triaxial transmitter.

enable a six-degrees-of-freedom (DOF) tracking, whereas only a five-DOF tracking is possible with uniaxial sensors.

Unfortunately, no reliable analytical (noniterative) methods for magnetic tracking of biaxial sensors seem to be described in literature. The present work is aimed at bridging this gap.

II. NONITERATIVE MAGNETIC TRACKING IN THREE-DIMENSIONAL (3-D) SPACE

Magnetic tracking in 3-D space can be based on simple and fast analytical procedures [3], [4] if the vector outputs of the receiver (magnetic sensor) can be combined into an orientation invariant scalar signal that is proportional to the total field magnitude at the sensor's location. In this case, the sensor location can be calculated first by processing the scalar signals received
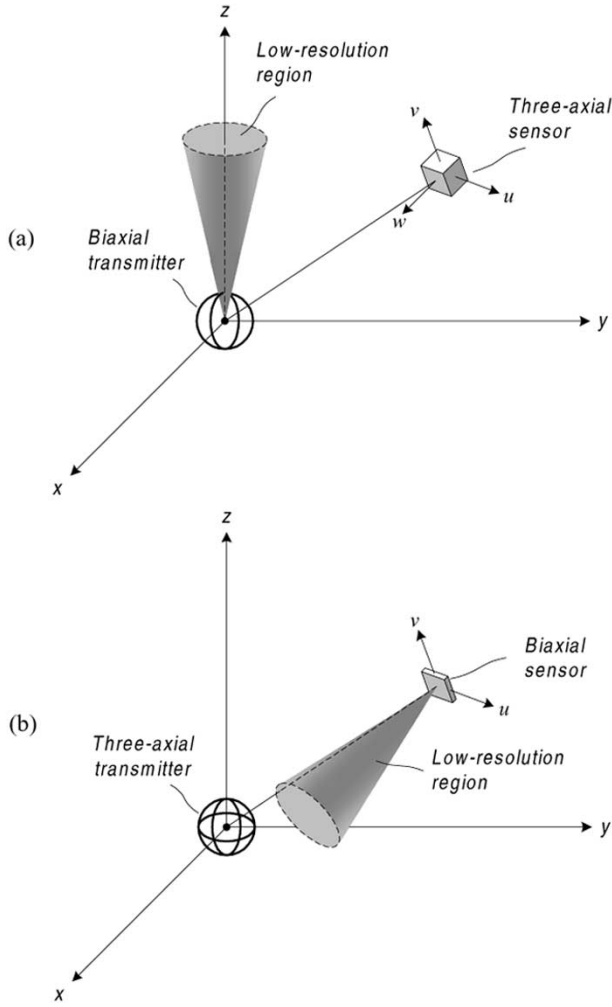
Fig. 2. Magnetic tracking reliability. (a) It is possible to limit location freedom of the sensor, and it can avoid the low-resolution region near the biaxial transmitter axis. (b) It is generally impossible to limit orientation freedom of the sensor, and the transmitter cannot avoid the reciprocal low-resolution region near the sensor's axis. (Not all low-resolution regions are shown in this figure.)

from different transmitters; then, the sensor's orientation can be found with reference to the known total field vectors at the sensor's location.

It is apparent that the simplest sensor suitable for the above procedure should be a triaxial one to supply both the vector and scalar outputs. The simplest transmitter can be a biaxial one. Such a transmitter provides enough information for localizing a triaxial sensor in a given quadrant of space [3], [4].

Reciprocity requires that the magnetic coupling remains the same if the sensor and the transmitter replace each other. Hence, it seems possible, *at first sight*, to localize a biaxial sensor with a triaxial transmitter [see Fig. 1(b)] by measuring the coupling between the transmitting and the sensing coils and then solving the reciprocal problem [3].

However, the difficulty is that there are low-resolution regions (LRRs) around the transmitter. It is known, for example, that the location resolution of the tracking drastically decreases near the coordinate axes of a triaxial transmitter [3]. The similar LRRs should be expected for a biaxial transmitter as well [see Fig. 2(a)]. To make things worse, the LRR shown in Fig. 2(a)

cannot be reoriented like it can be done by electrically rotating the triaxial transmitter in [3].

It is possible to keep the triaxial sensor in Fig. 2(a) away from the LRRs by simply limiting its location freedom. However, entering an LRR is unavoidable while solving the reciprocal problem of tracking a biaxial sensor in Fig. 2(b). It is generally impossible to limit orientation freedom of the sensor and to avoid the situations where the transmitter is within one of the sensor's reciprocal LRRs.

It seems that the only way of maintaining the resolution at the acceptable level is to increase the number of transmitters and to locate them in such a pattern that at least one of the transmitters is always away from the sensor's reciprocal LRRs.

To decide on the number of transmitters needed and their spatial pattern, we should carefully investigate the reciprocal LRRs of a biaxial sensor.

III. LOW-RESOLUTION REGIONS OF A BIAXIAL SENSOR

Let us consider two different methods of magnetic tracking with biaxial transmitters, [3] and [4]. We shall find the LRRs of the transmitter. These regions will represent the *reciprocal* LRRs of a biaxial sensor. For the sake of simplicity and without loss of generality, we assume that the magnetic moment of the transmitting coils $M = 2\pi$ A·m^2 and the sensor is located on a unit (1-m radius) spherical segment, as shown in Fig. 3(a).

According to method [3], the x- and y-axis transmitting coils [coil #1 and coil #2 in Fig. 3(a)] are excited in sequence by ac current of frequency ω. The sensor's location is found by processing the corresponding quasi-static magnetic dipole field amplitudes H_1, H_2 and their dot product $(H_1 \cdot H_2)$ seen by the sensor (indexes 1 and 2 are related here to transmitting coils #1 and #2, correspondingly)

$$\begin{cases} H_1^2 = x^2 + \dfrac{1}{4}y^2 + \dfrac{1}{4}z^2 \\ H_2^2 = \dfrac{1}{4}x^2 + y^2 + \dfrac{1}{4}z^2 \\ (H_1 \cdot H_2) = \dfrac{3}{4}xy \end{cases} \qquad (1)$$

where the scalar signals H_1^2, H_2^2, and $(H_1 \cdot H_2)$ are combined from the sensor vector outputs, such that

$$\begin{cases} H_1^2 = H_{1u}^2 + H_{1v}^2 + H_{1w}^2 \\ H_2^2 = H_{2u}^2 + H_{2v}^2 + H_{2w}^2 \\ (H_1 \cdot H_2) = H_{1u}H_{2u} + H_{1v}H_{2v} + H_{1w}H_{2w} \end{cases} . \qquad (2)$$

Solution of (1) gives the sensor's coordinates

$$\begin{cases} x = \sqrt{\dfrac{2}{3}}\sqrt{H_1^2 - H_2^2 + \sqrt{(H_1^2 - H_2^2)^2 + 4(H_1 \cdot H_2)^2}} \\ y = \dfrac{2\sqrt{\dfrac{2}{3}}(H_1 \cdot H_2)}{\sqrt{H_1^2 - H_2^2 + \sqrt{(H_1^2 - H_2^2)^2 + 4(H_1 \cdot H_2)^2}}} \\ z = \sqrt{2}\sqrt{H_1^2 + H_2^2 - \dfrac{5}{4}(x^2 + y^2)} \end{cases} . \qquad (3)$$

TABLE I
SIGNAL-TO-NOISE RATIO CALCULATION

Transmitting coils*			
	average diameter	9	cm
	number of turns	200	
	wire diameter	0.7	mm
	resistance	6	Ω
	exciting current	2	A z-p
	magnetic moment	1.5	Am^2
	excitation frequency	20	kHz
Sensing coils			
	average diameter	8	mm
	number of turns	2000	
	wire diameter	50	μm
	resistance	456	Ω
	inductance	68	mH
	tuning capacitance	1	nF
	quality factor	10	
Maximum signal detected at a 1 m distance		52	mV z-p
Bandwidth		200	Hz
Sensor coil thermal noise		390	nV rms
Preamplifier noise		57	nV rms
Atmospheric noise measured in a 1 Hz bandwidth		0.05	μA/m
Atmospheric noise measured at the amplifier input		112	nV rms
Total noise measured at the amplifier input		405	nV rms
Signal-to-noise ratio		>100	dB

*The transmitter noise is neglected because its amplitude component is small relative to the signal level; and its phase component can be effectively eliminated due to synchronous detection of the sensor outputs.
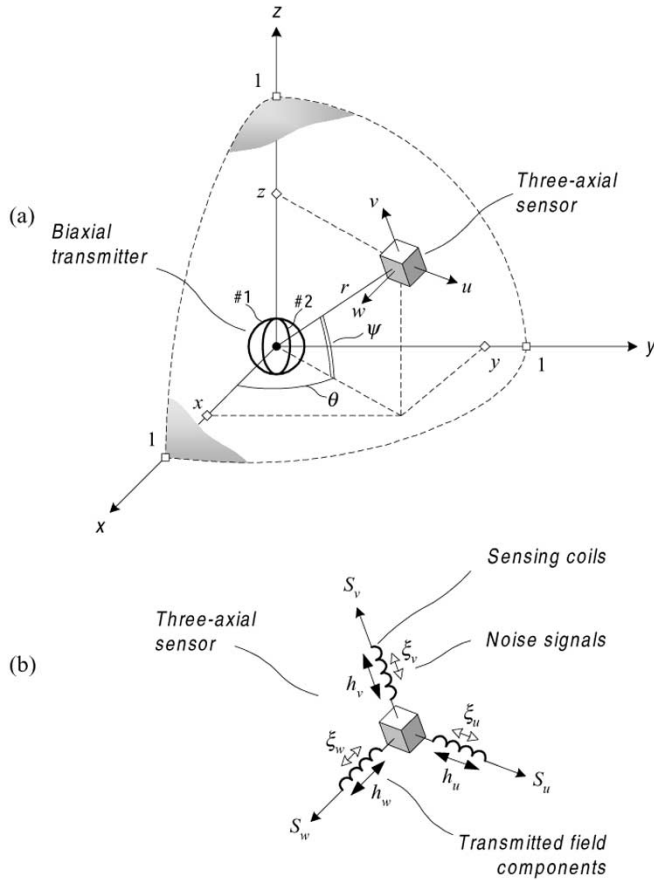
Fig. 3. Magnetic sensor location and structure. (a) Magnetic sensor is located at a fixed distance $r = 1$ m from the transmitter. Note that $z = \sqrt{1 - x^2 - y^2}$. (b) Independent noise signals ξ_v, ξ_u, ξ_w are superimposed on the corresponding sensor vector outputs S_v, S_u, S_w.

According to method [4], the transmitting coils are excited in quadrature at a quasi-static frequency ω, and the sensor's location is found as follows:

$$\begin{cases} r = \sqrt[3]{\dfrac{1}{2}\dfrac{1}{\sqrt{H_{\min}^2}}} \\ \theta = 0.5 \arctan \dfrac{2(H_1 \cdot H_2)}{H_{\max}^2 - H_{\min}^2} \\ \psi = \sqrt{\dfrac{1}{3}\left(\dfrac{H_{\max}^2}{H_{\min}^2} - 1\right)} \end{cases} \quad (4)$$

where r is the distance between the transmitter and the sensor, θ is the azimuth, and ψ is the elevation angle [see Fig. 3(a)], such that

$$\begin{cases} x = r \cos\psi \cos\theta \\ y = r \cos\psi \sin\theta \\ z = r \sin\psi \end{cases} \quad (5)$$

The azimuth θ and the total field extremes in (4)

$$H_{\max}^2 = 0.5 \left[H_1^2 + H_2^2 + \sqrt{4(H_1 \cdot H_2)^2 + (H_1^2 - H_2^2)^2} \right] \quad (6)$$

$$H_{\min}^2 = 0.5 \left[H_1^2 + H_2^2 - \sqrt{4(H_1 \cdot H_2)^2 + (H_1^2 - H_2^2)^2} \right] \quad (7)$$

can be found by analyzing the following equation for the total scalar field seen by the sensor:

$$\begin{aligned} h^2 = &(H_{1u}\cos\varpi t + H_{2u}\sin\varpi t)^2 \\ &+ (H_{1v}\cos\varpi t + H_{2v}\sin\varpi t)^2 \\ &+ (H_{1w}\cos\varpi t + H_{2w}\sin\varpi t)^2. \end{aligned} \quad (8)$$

The field components H_1 and H_2 in (4), (6), and (7) can be extracted from the sensor total output with the help of synchronous detection.

To determine the LRRs of the biaxial transmitter in Fig. 3(a), we suppose that independent noise signals $\xi_v, \xi_u,$ and ξ_w are superimposed on the corresponding sensor vector outputs [see Fig. 3(b)]. We also suppose that root-mean-square (rms) values of the above noise signals are equal $\sigma_u = \sigma_v = \sigma_w = \sigma_n$ and weak $(1/10^5)$ relative to the maximum magnitude of the sensor vector outputs (see a practical case in Table I).

We can now find the resolution $\sigma_{(x,y,z)}$ of methods [3] and [4] as a function of the sensor's location (x, y, z) on the spherical surface in Fig. 3(a)

$$\sigma_{(x,y,z)} = \sqrt{\sigma_x^2 + \sigma_y^2 + \sigma_z^2} \quad (9)$$

where $\sigma_x, \sigma_y,$ and σ_z are the rms estimation errors of the corresponding sensor's coordinates.

The σ_x, σ_y, and σ_z errors can be determined with the help of Gauss's error propagation rule. Equation (3) suggests the following system of partial derivatives for method [3]:

$$\begin{cases} \sigma_x^2 = \left(\dfrac{\partial x}{\partial H_1^2}\sigma_{H_1^2}\right)^2 + \left(\dfrac{\partial x}{\partial H_2^2}\sigma_{H_2^2}\right)^2 \\ \qquad + \left[\dfrac{\partial x}{\partial (H_1 \cdot H_2)}\sigma_{(H_1 \cdot H_2)}\right]^2 \\ \sigma_y^2 = \left(\dfrac{\partial y}{\partial H_1^2}\sigma_{H_1^2}\right)^2 + \left(\dfrac{\partial y}{\partial H_2^2}\sigma_{H_2^2}\right)^2 \\ \qquad + \left[\dfrac{\partial y}{\partial (H_1 \cdot H_2)}\sigma_{(H_1 \cdot H_2)}\right]^2 \\ \sigma_z^2 = \left(\dfrac{\partial z}{\partial H_1^2}\sigma_{H_1^2}\right)^2 + \left(\dfrac{\partial z}{\partial H_2^2}\sigma_{H_2^2}\right)^2 \\ \qquad + \left[\dfrac{\partial z}{\partial (H_1 \cdot H_2)}\sigma_{(H_1 \cdot H_2)}\right]^2 \end{cases}. \quad (10)$$

Equation (5) suggests the following system of partial derivatives for method [4]:

$$\begin{cases} \sigma_x^2 = \left(\dfrac{\partial x}{\partial r}\sigma_r\right)^2 + \left(\dfrac{\partial x}{\partial \theta}\sigma_\theta\right)^2 + \left(\dfrac{\partial x}{\partial \psi}\sigma_\psi\right)^2 \\ \sigma_y^2 = \left(\dfrac{\partial y}{\partial r}\sigma_r\right)^2 + \left(\dfrac{\partial y}{\partial \theta}\sigma_\theta\right)^2 + \left(\dfrac{\partial y}{\partial \psi}\sigma_\psi\right)^2 \\ \sigma_z^2 = \left(\dfrac{\partial z}{\partial r}\sigma_r\right)^2 + \left(\dfrac{\partial z}{\partial \psi}\sigma_\psi\right)^2 \end{cases} \quad (11)$$

where

$$\begin{cases} \sigma_r^2 = \left(\dfrac{\partial r}{\partial H_1^2}\sigma_{H_1^2}\right)^2 + \left(\dfrac{\partial r}{\partial H_2^2}\sigma_{H_2^2}\right)^2 \\ \qquad + \left[\dfrac{\partial r}{\partial (H_1 \cdot H_2)}\sigma_{(H_1 \cdot H_2)}\right]^2 \\ \sigma_\theta^2 = \left(\dfrac{\partial \theta}{\partial H_1^2}\sigma_{H_1^2}\right)^2 + \left(\dfrac{\partial \theta}{\partial H_2^2}\sigma_{H_2^2}\right)^2 \\ \qquad + \left[\dfrac{\partial \theta}{\partial (H_1 \cdot H_2)}\sigma_{(H_1 \cdot H_2)}\right]^2 \\ \sigma_\psi^2 = \left(\dfrac{\partial \psi}{\partial H_1^2}\sigma_{H_1^2}\right)^2 + \left(\dfrac{\partial \psi}{\partial H_2^2}\sigma_{H_2^2}\right)^2 \\ \qquad + \left[\dfrac{\partial \psi}{\partial (H_1 \cdot H_2)}\sigma_{(H_1 \cdot H_2)}\right]^2 \end{cases}. \quad (12)$$

To evaluate the rms noise magnitudes $\sigma_{H_1^2}$, $\sigma_{H_2^2}$, and $\sigma_{(H_1 \cdot H_2)}$ of the sensor scalar outputs H_1^2, H_2^2, and $(H_1 \cdot H_2)$, we neglect the second-order noise terms in the following equations for the corresponding noise signals:

$$\begin{aligned} \xi_{H_1^2} &= (H_{1u} + \xi_u)^2 + (H_{1v} + \xi_v)^2 \\ &\quad + (H_{1w} + \xi_w)^2 - \left(H_{1u}^2 + H_{1v}^2 + H_{1w}^2\right) \\ &\approx 2H_{1u}\xi_u + 2H_{1v}\xi_v + 2H_{1w}\xi_w \end{aligned} \quad (13)$$
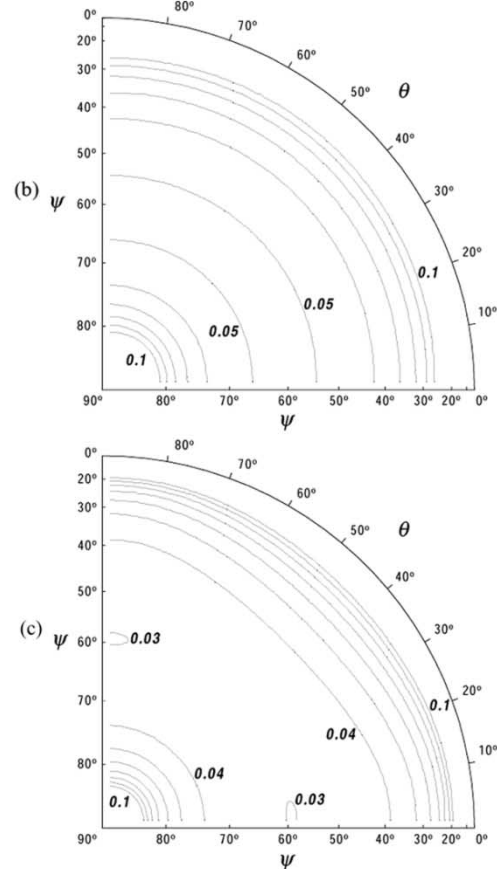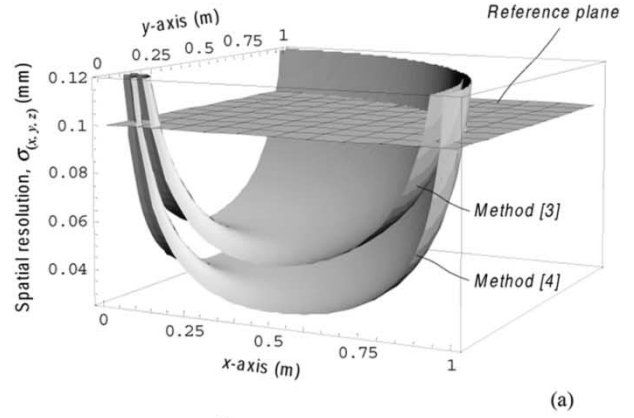

Fig. 4. Location resolution $\sigma_{(x,y,z)}$ calculated for the sensor in Fig. 3(a) as a function of the sensor's coordinates x and y in (a) and as a function of θ and ψ (contour plots) for method [3] in (b) and method [4] in (c). The bold numbers in parts (b) and (c) represent the location resolution, $\sigma_{(x,y,z)}$, measured in millimeters.

and

$$\begin{aligned} \xi_{(H_1 \cdot H_2)} &= (H_{1u} + \xi_u)(H_{2u} + \xi_u) \\ &\quad + (H_{1v} + \xi_v)(H_{2v} + \xi_v) \\ &\quad + (H_{1w} + \xi_w)(H_{2w} + \xi_w) \\ &\quad - (H_{1u}H_{2u} + H_{1v}H_{2v} + H_{1w}H_{2w}) \\ &\approx H_{1u}\xi_u + H_{2v}\xi_v + H_{1w}\xi_w \\ &\quad + H_{2u}\xi_u + H_{1v}\xi_v + H_{2w}\xi_w. \end{aligned} \quad (14)$$

We now can write according to (13)

$$\begin{aligned} \sigma_{H_1^2} &\approx \sqrt{(2H_{1u}\sigma_u)^2 + (2H_{1v}\sigma_v)^2 + (2H_{1w}\sigma_w)^2} \\ &= 2\sigma_n\sqrt{H_1^2} \end{aligned} \quad (15)$$
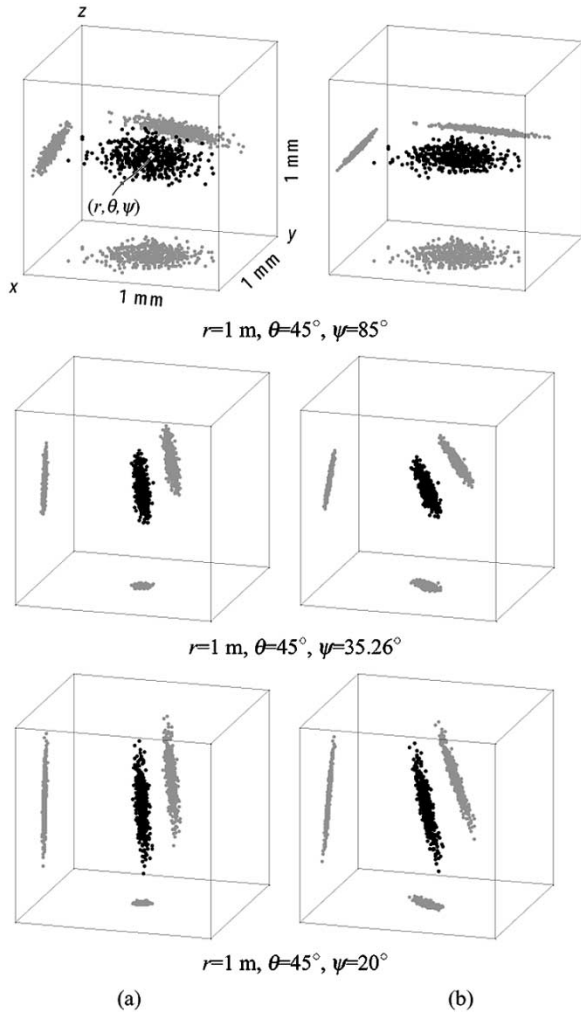
Fig. 5. Simulation of the sensor's location estimates for $r = 1$ m, $\theta = 45°$ and different ψ under noise conditions $\sigma_n = 10^{-5}$ (a) according to (3) and (b) according to (4). Each cube corresponds to a $1 \times 1 \times 1$ mm area around the true sensor's location. The black dots within the cubes are the location estimations (500 total for each cube). The gray dots on the cubes' facets are projections of the dots within the cube.
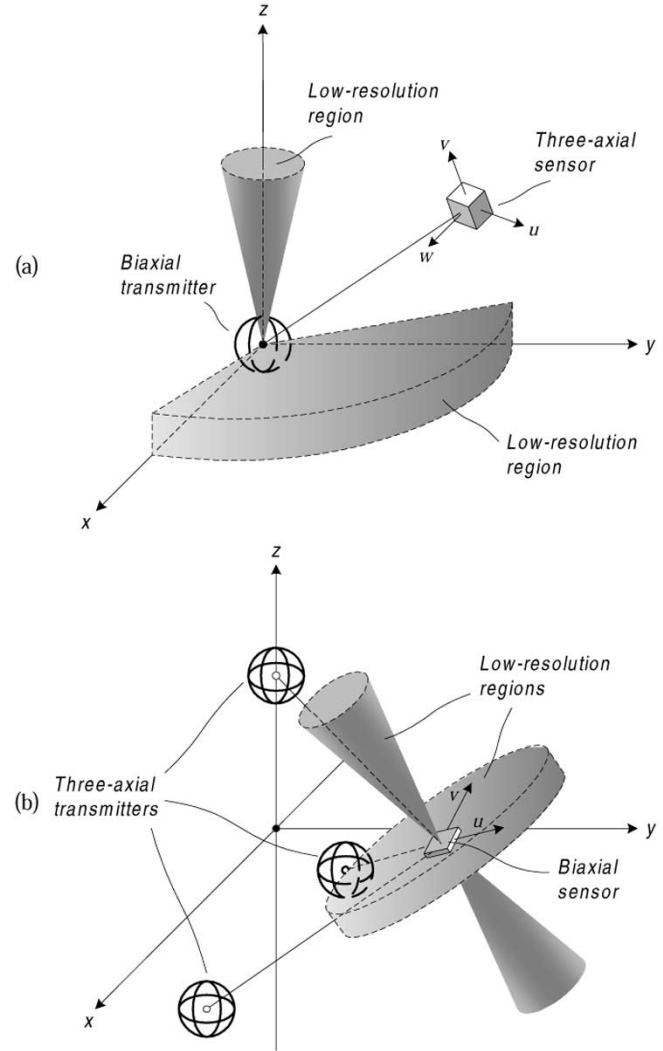

Fig. 6. Magnetic tracking errors. (a) The triaxial sensor can avoid the low-resolution regions related to the biaxial transmitter. (b) While solving the reciprocal problem, a triad of the triaxial transmitters cannot always avoid the reciprocal low-resolution regions related to the biaxial sensor.

and in the same way

$$\sigma_{H_2^2} \approx 2\sigma_n \sqrt{H_2^2}. \tag{16}$$

According to (14)

$$
\begin{aligned}
\sigma_{(H_1 \cdot H_2)} &\approx \big[(H_{1u}\sigma_u)^2 + (H_{1v}\sigma_v)^2 \\
&\quad + (H_{1w}\sigma_w)^2 + (H_{2u}\sigma_u)^2 \\
&\quad + (H_{2v}\sigma_v)^2 + (H_{2w}\sigma_w)^2 \big]^{1/2} \\
&= \sigma_n \sqrt{H_1^2 + H_2^2}.
\end{aligned} \tag{17}
$$

Substitution of $\sigma_{H_1^2}, \sigma_{H_2^2}$, and $\sigma_{(H_1 \cdot H_2)}$ from (13)–(15) into (10), (11) and taking the derivatives yield the location resolution $\sigma_{(x,y,z)}$ of methods [3] and [4].

Fig. 4(a) shows the resolution $\sigma_{(x,y,z)}$ as a function of the sensor's coordinates x and y. Fig. 4(b) and (c) show contour plots of the $\sigma_{(x,y,z)}$ as a function of the azimuth θ and elevation ψ angles. Fig. 5 shows the simulation of the sensor's location estimates for a $\theta = 45°$ and different values of ψ.

As seen from Figs. 4 and 5, the location resolution of both methods [3] and [4] rapidly degrades when coordinate z approaches either zero or unity.

Fig. 4(b) and (c) shows that the elevation angle ψ should be $27° < \psi < 81°$ for method [3] and $19° < \psi < 84°$ for method [4] to provide a resolution $\sigma_{(x,y,z)} < 0.1$ mm rms in a 200-Hz bandwidth (see Table I).

The elevation angles ψ that are beyond the above limits represent the LRRs of the biaxial transmitter [see Fig. 6(a)]. Similar LRRs should be related to the biaxial sensor while solving the reciprocal problem [see Fig. 6(b)].

Fig. 6(b) makes it clear that the triad of transmitters cannot always avoid the reciprocal LRRs of the sensor. At least one more transmitter should be added to the transmitting array for a reliable tracking.

IV. TRACKING WITH A TRIAD OF TRANSMITTERS

Rather than to raise the number of transmitters in Fig. 6(b) beyond three, it is worth examining the resolution of the distance r estimation by each of the transmitters. Three different and reliable distance estimates obtained with a triad of transmitters [see

The r^2 estimation error can be evaluated assuming that the sensor coordinates are measured with independent errors ξ_x, ξ_y, ξ_z and neglecting the second-order terms

$$\begin{aligned}\xi_{r^2} &= (x + \xi_x)^2 + (y + \xi_y)^2 + (z + \xi_z)^2 \\ &\quad - x^2 - y^2 - z^2 \\ &\approx 2x\xi_x + 2y\xi_x + 2z\xi_x.\end{aligned} \quad (19)$$

The rms value of the r^2 estimation error can be found then as

$$\sigma_{r^2} \approx \sqrt{(2x\sigma_x)^2 + (2y\sigma_y)^2 + (2z\sigma_z)^2} \quad (20)$$

which, considering (10) and (15)–(17), leads to

$$\begin{aligned}\sigma_{r^2} &\approx \frac{2}{3}\sqrt{38}\sigma_n \sqrt{2 + 3(x^2 + y^2)} \\ &\approx 4\sigma_n \sqrt{2 + 3(x^2 + y^2)}.\end{aligned} \quad (21)$$

Since

$$r + \sigma_r = \sqrt{r^2 + \sigma_{r^2}}\big|_{r \neq 1} \approx r + \frac{1}{2r}\sigma_{r^2} \quad (22)$$

then the rms value of the distance estimation error, or the distance resolution, can be written as

$$\sigma_r\big|_{r=1} \approx \frac{1}{2}\sigma_{r^2} \approx 2\sigma_n \sqrt{2 + 3(x^2 + y^2)}. \quad (23)$$

For method [4], the distance resolution can be found from (12) and (22) as follows:

$$\sigma_r\big|_{r=1} = \frac{2}{3}\sigma_n \sqrt{1 + 6\frac{x^2 y^2}{x^2 + y^2}}. \quad (24)$$

Comparison between (23) and (24) suggests that the distance resolution of method [4] is at least four times better than that of method [3].

Examination of (24) shows that for method [4] $\sigma_r < 0.01$ mm for any location of the sensor on the unit radius sphere in Fig. 3(a). In other words, there are no LRRs for the distance estimation. As a result, it is always possible to localize (triangulate) a biaxial sensor with a triad of triaxial transmitters.

It is quite obvious that the triangulation resolution $\sigma_{(x,y,z)}$ depends on the distance between the transmitters in the triad and the distance between the triad and the sensor [see Fig. 7(a)]. A simulation of the sensor location estimates is shown in Fig. 7(b) for the triad where the transmitters are uniformly situated on a circle of a 0.3 m radius.

A comparison of Fig. 7(b) against Fig. 5 shows a two- to threefold improvement in the location resolution. It means that the increase in the total number of transmitters from one biaxial transmitter in Fig. 1(a) to three triaxial transmitters in Fig. 7(a) will not finally demand decreasing the update rate of the location estimation. To keep the same update rate of the location estimation, each of the nine transmitting coils in Fig. 7(a) should be operated during the time intervals that are by a factor of 4.5 shorter than the time intervals of operating the two transmitting coils in Fig. 1(a). This increases by the same factor both the signal and noise bandwidth. As a result, the location resolution shown in Fig. 7(b) will be reduced by a factor of $\sqrt{4.5}$, assum-ing that the magnitude of transmitted signals is kept constant (despite reducing their duty cycle) and the noise interfering the system is white. The above reduction will equal the location
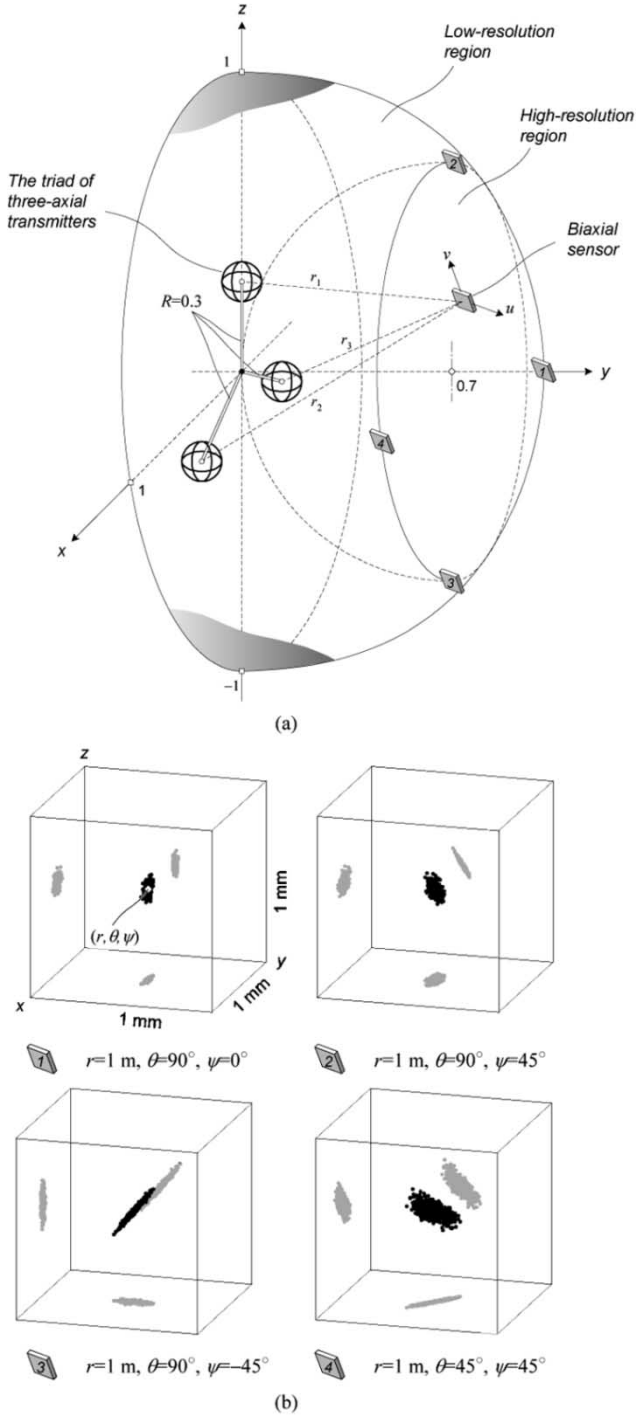

Fig. 7. Magnetic tracking with a triad of transmitters. (a) Magnetic sensor is located at a fixed distance $r = 1$ m from the triad of transmitters. (b) Simulation of the sensor's location estimates under noise conditions $\sigma_n = 10^{-5}$. Each cube corresponds to a $1 \times 1 \times 1$ mm area around the true sensor's location. The dots within the cubes are the location estimations (500 dots total for each cube).

Fig. 7(a)] will be enough to localize the sensor with triangulation technique.

For method [3], the distance between the transmitter and the sensor [see Fig. 3(a)] is related to the sensor's coordinates as follows:

$$r^2 = x^2 + y^2 + z^2. \quad (18)$$

resolution of the tracking with the triad of triaxial transmitters to that of a biaxial transmitter, provided that in both cases the location update rate is the same.

V. CONCLUSION

The investigation of the LRRs of a biaxial transmitter helped us determine the *reciprocal* LRRs of a biaxial sensor. The regions configuration suggested employing at least four triaxial transmitters for reliable tracking. The investigation of the resolution of the distance between the sensor and the transmitter revealed that no LRRs exist in this case. Hence, it is possible to localize the biaxial sensor with a triad of transmitters with the help of triangulation.

It is shown that method [4] provides a better distance resolution and, therefore, a better location resolution of the triangulation than method [3] does. It is also shown that the location resolution of the new triangulation technique is nearly equal to that obtained in [3] and [4] for the same system's update rate and magnitude of the signals transmitted. It is so despite the need to operate a greater number of transmitting coils.

It is interesting to note that in the case where transmitting coils are operated at their maximum active power (reed temperature), the location resolution of the proposed method can be from two to three times better than that of methods [3] and [4]. The signal magnitude in this case is in inverse proportion to the square root of the signal's duty cycle. The signal bandwidth and therefore the noise also are in the same relation to the signal's duty cycle. As a result, the signal-to-noise ratio is not degraded when the transmitting signals' duty cycle is decreased in order to operate more transmitting coils during the same update period.

It is also interesting to note that in the above case time-sharing operation of the transmitting coils provides not worse signal-to-noise ratio than frequency-sharing one.

In this work, we have not treated the tracking of the sensor's orientation assuming that it can be quite easily computed after the sensor location is found. The computation algorithms can be based on [3] or [4].

REFERENCES

[1] Ascension Technology Corporation Products Application [Online]. Available: http://www.ascension-tech.com/products/minibird/
[2] G. Perry, private communication, 2002.
[3] F. H. Raab, "Remote Object and Orientation Locator," U.S. Patent 4 314 251, Feb. 1982.
[4] E. Paperno, I. Sasada, and E. Leonovich, "A new method for magnetic position and orientation tracking," *IEEE Trans. Magn.*, vol. 37, pp. 1938–1940, July 2001.